Available online at www.sciencedirect.com

ScienceDirect

www.elsevier.com/locate/jes

JES JOURNAL OF ENVIRONMENTAL SCIENCES

www.jesc.ac.cn

Quantitative structure-activity relationship in the photodegradation of azo dyes

Guoyang Zhang, Shujuan Zhang *

State Key Laboratory of Pollution Control and Resource Reuse, School of the Environment, Nanjing University, Nanjing 210023, China

ARTICLE INFO

Article history:
Received 8 September 2019
Received in revised form
7 November 2019
Accepted 11 November 2019
Available online 9 December 2019

Keywords:
Azo
Hydrazone
Photolysis
QSAR
Softness

ABSTRACT

The photolysis characteristics of azo dyes are critically important in environmental pollution control, dye-sensitized solar cells, and dyeing-related industries. However, there is still lack of quantitative relationship between the structures of azo dyes and their photolysis characteristics. To address this issue, the photolysis of 22 azo dyes were conducted side by side at three pH (4.0, 6.0, 9.0). The obtained pseudo-first order photodegradation rate constants (k_1) were processed with meta-analysis. Statistically, the hydrazone tautomer had a smaller excitation energy and was easier to undergo photolysis than the azo tautomer. The *ortho*-substituted sulfonate groups had an obvious protective effect on the photostability of azo dyes. The softness (s), the most positive and negative partial charge on a carbon atom (qC^+, qC^-) were found to be crucial descriptors in the establishment of QSAR models for the photostability of azo dyes. The QSAR model at pH 9.0 was robust for predicting the photostability of azo dyes under UV irradiation. N_2-purging experiments and quantum chemical computation verified that the cleavage of azo bond was not a result of direct photolysis but was caused by the attack of photoinduced reactive oxygen species. The results here are helpful for the design of more stable azo dyes or the selection of suitable approaches for the treatment of dye-contaminated water bodies.

Introduction

Azo dyes are the largest class of chemically synthesized dyes, and are widely used in textile dyeing, leathering, food processing, cosmetics, and paper printing (Pandey et al., 2007). Due to the recalcitrant nature of synthetic dyes, the disposal of wastewater from the above industries is a difficult task in the field of environmental protection. Conventional treatment methods, such as flocculation, chemical oxidation and biodegradation, can only remove 70–80% of the effluent dyes (Al-Kdasi et al., 2004; Thanavel et al., 2019). The residual azo dyes in the waste streams would be a significant threat to public health and ecological environment (Chung, 2016; Puvaneswari et al., 2006; Sztandera et al., 2003). Photolysis is one of the dominant transformation pathways of dyes in natural environment. In recent decades, UV-based advanced oxidation processes (AOPs), such as UV/H_2O_2, UV/ozone, UV/chlorine, UV/Fenton, and UV/TiO_2, have been extensively investigated for the elimination of

* *Corresponding author.*
E-mail address: sjzhang@nju.edu.cn (S. Zhang).

https://doi.org/10.1016/j.jes.2019.11.009

dyestuffs (Abo-Farha, 2010; Chan et al., 2011; Katsumata et al., 2010; Soares et al., 2016; Wu et al., 2016; Yasar et al., 2007). Except for being studied as target compounds for the purpose of pollution control, azo dyes are also widely used as probing molecules in the performance evaluation of emerging photocatalysts (Anwer et al., 2019; Chen et al., 2017; Ma et al., 2019), or used as photosensitizers in many photoelectrochemical systems, such as dye-sensitized solar cells (DSSCs) (Basheer et al., 2018; Ekmekci et al., 2019; Sato et al., 2018). In UV-based AOPs, we are trying to take the advantage of the self-photolysis of dyes, whereas the photostability of dyes is a crucial factor that determines the efficiency of DSSCs.

The photolysis/photostability of dyes is highly dependent on the chemical structures and solvent circumstance. Azo dyes are characterized by nitrogen to nitrogen double bonds (–N=N–) that are usually attached to two aromatic rings (benzene or naphthalene). When irradiated with UV light, the azo dyes would undergo photochemical *cis-trans* isomerization (Brode et al., 1952), photosensitized oxidation (Kuramoto and Kitao, 1982a), one-electron oxidation (Coen et al., 2001) and photoreduction process (van Beek et al., 1971; van Beek and Heertjes, 1963). However, the relationship between the photolytic characteristics of azo dyes and their molecular structures has not been thoroughly explored (Beiknejad and Chaichi, 2014; Haag and Mill, 1987; Kuramoto and Kitao, 1982; van Beek and Heertjes, 1963).

Quantitative structure activity relationship (QSAR) is a cost-effective and powerful tool that helps to get insight into the reaction mechanisms (Mannhold et al., 2008). Lots of QSARs have been developed for predicating photochemical quantum yields, half-lives or reactivity of chemicals, on the basis of certain quantum chemical parameters, such as the energy of the highest occupied molecular orbital (E_{HOMO}), the energy of the lowest unoccupied molecular orbital (E_{LUMO}), hardness (η) and softness (s) (Chen et al., 2000, 2001; Sudhakaran and Amy, 2013; Xiao et al., 2015). Beiknejad et al. found that the photolysis half-lives of dyes depended strongly on E_{HOMO}, the largest electron density of an atom in the molecule (ED^+) and the lipophilicity (log$P$) (Beiknejad and Chaichi, 2014). However, the data set included only 4 azo dyes and could not describe the photochemical characteristics of overall azo dyes. On the other hand, solution pH affects the speciation of azo dyes, and consequently influences the photochemical properties, which are rarely considered in previous QSAR studies (Beiknejad and Chaichi, 2014).

The objective of this study is to address the unclear issues in the relationship between the structures of azo dyes and the photolysis characteristics. First, we collected a data set consisting 22 azo dyes through the photolysis experiments side-by-side at three pHs (4.0, 6.0, 9.0). A meta-analysis was conducted to understand the role of functional groups and conjugated systems in the photostability of azo dyes. Second, the molecular structure parameters of these azo dyes were calculated with the density functional theory (DFT). Correlation analysis, principal component analysis (PCA), and multilinear regression (MLR) were used to develop QSAR models at the three pHs (4.0, 6.0, 9.0). Internal and external validations were conducted to check the robustness and predictability of these models.

1. Materials and methods

1.1. Materials

All the azo dyes were obtained from Sinopharm Chemical Reagent Co. Ltd., China or TCI (Shanghai) Development Co. Ltd., China. Molecular structures and CAS numbers of the 22 dyes were shown in Fig. 1. These azo dyes can be divided into two major categories: hydroxyazo dyes and aminoazo dyes. The azo coupling in the first category usually takes place at the *ortho*- or *para*-position to the hydroxyl group, while that in the second category usually occurs at the position to the amino group. The hydroxyazo dyes exist as azo-hydrazone tautomerism (Ball and Nicholls, 1982), while the aminoazo dyes exist exclusively as azo tautomers. The diazo dyes (Ponceau S, Naphthol Blue Black and Acid Red 73) containing amino and hydroxyl groups are counted in the stack for these two categories.

NaOH and $HClO_4$ of analytical grade were obtained from Nanjing Reagent Station, China. Ultrapure water (18.25 MΩ cm) made from a water purification system (Shanghai Ulupure Industrial Co., Ltd., China) were used for the preparation of sample solutions. High purity N_2 (99.999%) was purchased from Nanjing Tianze Gas Co., Ltd., China.

1.2. Irradiation experiments

UV irradiation experiments were carried out in a rotating disk photoreactor (Nanjing StoneTech Electric Equipment, China) with a 300 W medium-pressure mercury lamp (MP-Hg, Shanghai Hongguang Tungsten & Molybdenum Technology Co., Ltd.) of maximum emission at 365 nm as the light source. The diagrammatic sketch of the photo-reactor has been reported in our previous work (Zhang et al., 2018). The light intensity was measured with a radiometer (Photoelectric Instrument Factory of Beijing Normal University, China) equipped with a sensor of peak sensitivity at 365 nm. Sample solutions (25 mL) containing 100 μmol/L target dye were parallelly arranged in a quartz tube around the lamp. The initial solution pH was adjusted to the needed value with $HClO_4$ and NaOH. In N_2-purged experiments, the sample solutions were firstly purged with N_2 for 30 min prior to irradiation and then continuously purged during photo-irradiation.

UV-Vis spectra of raw and irradiated dye solutions were recorded with a double beam spectrophotometer (UV-2700, Shimadzu, Japan). The dye concentrations were detected with the UV spectrophotometer at their maximum absorption wavelengths.

The photodegradation of these azo dyes followed pseudo-first-order kinetics:

$$-dC/dt = k_1 C \quad (1)$$

where k_1 is the pseudo-first-order decolorization constant and C is the concentration of dye. Integration of

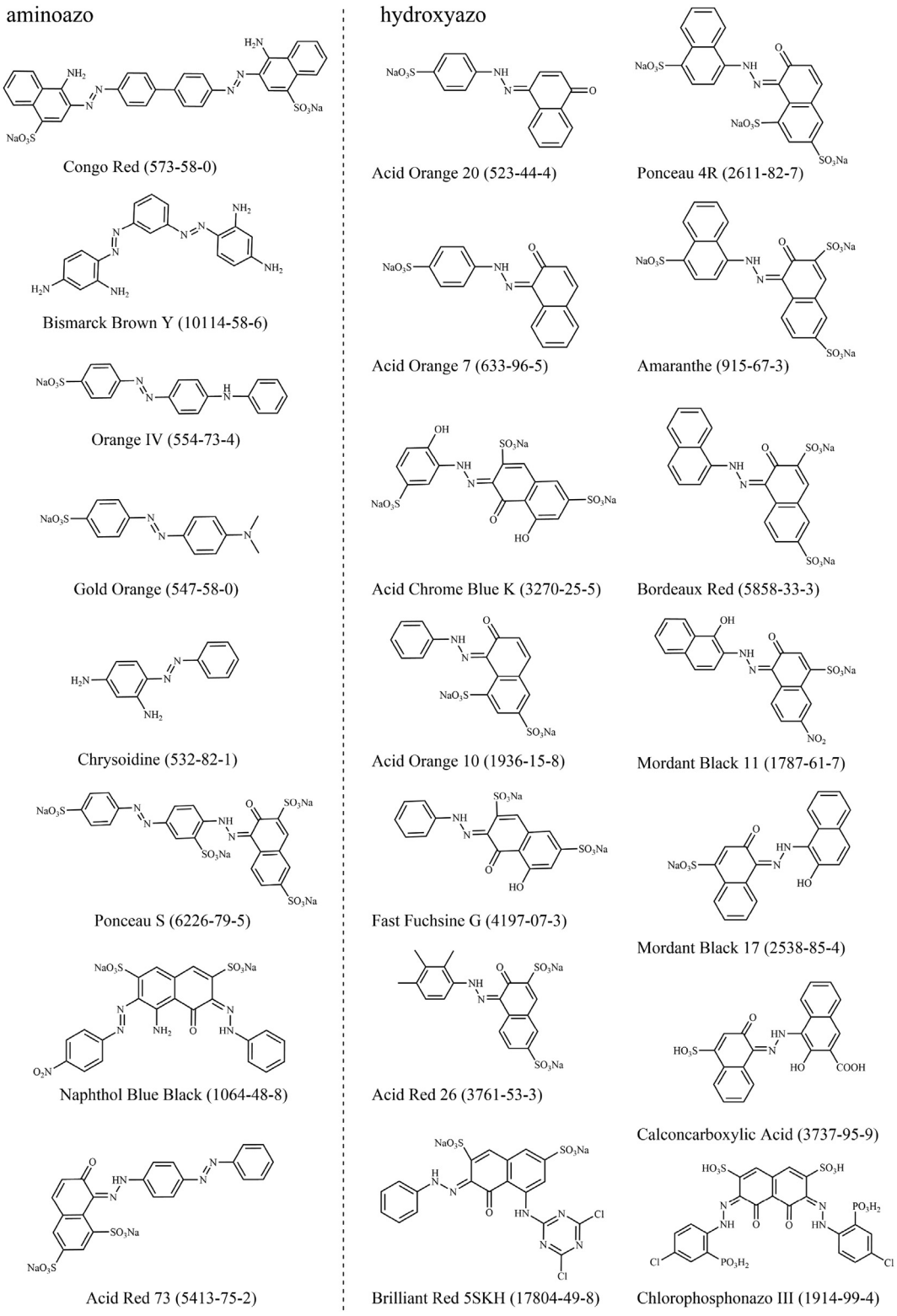

Fig. 1 – Molecular structure of the azo dyes.

Equation (1) results in a linear dependency of ln (C_0/C) on t with a slope of k_1. The photolysis experiments for each azo dye were carried out at three pH values (4.0, 6.0, 9.0), respectively.

1.3. *Quantum chemical calculation*

The DFT quantum chemical calculations were carried out with Gaussian 09 (Frisch et al., 2010). Geometry optimizations

of dyes were performed using the B3LYP hybrid density functional and the 6-31 + G (d, p) basis set (Lee et al., 1988). The optimized structure were confirmed as true minima by calculating the harmonic vibrational frequencies at the same level. No imaginary vibrational frequency was observed for the optimized geometries. Solvent effects were introduced in the calculations considering an electrostatic influence with the SMD method (Marenich et al., 2009). The values of the all quantum chemical descriptors are listed in Table 1. The topological polar surface area (*PSA*), average polarizability (α), total dipole moment (μ), E_{HOMO}, E_{LUMO}, energy difference between LUMO and HOMO (E_{GAP}), the most positive/negative partial charge on a carbon atom (qC^+/qC^-), the most positive/negative partial charge on a hydrogen atom (qH^+/qH^-) were obtained from the Gaussian 09. Hardness (η), electronegativity (ζ), softness (s) and electrophilicity index (ω) were proven to be significant in QSAR/QSPR studies on the photolysis of chemicals (Chen et al., 1996; Pearson, 1986). According to Koopmans' theorem for closed-shell molecules, these four descriptors can be redefined as (Berkowitz and Parr, 1988; Zhan et al., 2003):

$$\eta = (IP - EA)/2 \quad (2)$$

$$\zeta = (IP + EA)/2 \quad (3)$$

$$s = 1/(IP - EA) \quad (4)$$

$$\omega = \zeta^2/(2\eta) \quad (5)$$

where *IP* was the vertical ionization potential, and *EA* was the vertical electron affinity. *IP* and *EA* were calculated from the absolute energies with Eqs. (6) and (7), respectively, in which M, M^+, and M^-, were the neutral, cationic, and anionic, forms of the optimized dye structures.

$$IP = E(M) - E(M^+) \quad (6)$$

Table 1 – The molecular descriptors of azo dyes.

Dyes	*PSA*	α	E_{HOMO}	E_{LUMO}	E_{GAP}	μ	*EA*	*IP*
Bismarck Brown Y	154	623.13	−5.348	−2.325	3.023	2.127	2.599	5.133
Acid Red 73	197	759.62	−5.980	−3.212	2.768	14.272	3.451	5.745
Chrysoidine	77	359.48	−5.398	−2.290	3.108	5.894	2.575	5.136
Gold Orange	94	464.29	−5.431	−2.538	2.893	13.115	2.810	5.149
Orange IV	102	666.15	−6.202	−3.473	2.729	23.440	3.743	5.977
Mordant Black 11[a]	173	705.24	−5.765	−3.292	2.473	19.152	3.541	5.512
Mordant Black 17	127	584.34	−5.597	−3.145	2.451	12.772	3.418	5.338
Acid Orange 7	107	438.45	−6.004	−2.908	3.096	5.828	3.183	5.749
Acid Orange 20	107	482.80	−5.818	−2.969	2.849	10.957	3.246	5.563
Calconcarboxylic Acid	162	637.63	−5.804	−3.404	2.401	9.874	3.673	5.551
Brilliant Red 5SKH[a]	223	695.81	−5.916	−3.199	2.717	8.274	3.460	5.666
Fast Fuchsine G	193	523.22	−6.032	−3.148	2.885	8.201	3.397	5.798
Acid Chrome Blue K	279	612.76	−5.856	−3.137	2.719	15.080	3.393	5.613
Amaranthe	238	660.70	−6.084	−3.386	2.698	6.864	3.650	5.841
Bordeaux Red	173	615.32	−5.811	−3.171	2.640	18.295	3.447	5.559
Acid Red 26[a]	173	563.26	−5.978	−3.158	2.820	14.353	3.426	5.735
Acid Orange 10	173	502.54	−6.052	−2.972	3.080	13.404	3.236	5.792
Ponceau 4R	242	612.63	−5.851	−2.724	3.127	12.5235	2.957	5.618
	η	s	ζ	ω	qC^-	qC^+	qH^-	qH^+
Bismarck Brown Y	1.267	0.395	3.866	5.897	−0.753	0.778	0.152	0.374
Acid Red 73	1.147	0.436	4.598	9.217	−1.645	0.585	0.172	0.409
Chrysoidine	1.281	0.390	3.856	5.805	−0.719	0.559	0.153	0.349
Gold Orange	1.170	0.428	3.980	6.771	−1.138	0.654	0.158	0.183
Orange IV	1.117	0.448	4.860	10.575	−0.971	1.019	0.169	0.211
Mordant Black 11[a]	0.985	0.507	4.527	10.397	−1.119	0.802	0.165	0.455
Mordant Black 17	0.960	0.521	4.378	9.982	−0.857	0.626	0.152	0.463
Acid Orange 7	1.283	0.390	4.466	7.774	−0.806	0.467	0.160	0.332
Acid Orange 20	1.158	0.432	4.404	8.372	−0.833	0.614	0.167	0.356
Calconcarboxylic Acid	0.939	0.532	4.612	11.323	−0.768	1.200	0.156	0.467
Brilliant Red 5SKH[a]	1.103	0.453	4.563	9.438	−1.840	1.025	0.167	0.409
Fast Fuchsine G	1.201	0.416	4.597	8.802	−1.477	1.259	0.169	0.463
Acid Chrome Blue K	1.110	0.450	4.503	9.130	−1.316	1.057	0.182	0.470
Amaranthe	1.095	0.456	4.746	10.279	−1.588	0.569	0.171	0.385
Bordeaux Red	1.056	0.473	4.503	9.600	−1.790	0.745	0.156	0.378
Acid Red 26[a]	1.154	0.433	4.580	9.089	−1.633	0.470	0.158	0.410
Acid Orange 10	1.278	0.391	4.514	7.973	−1.561	0.911	0.163	0.409
Ponceau 4R	1.331	0.376	4.287	6.908	−1.660	0.538	0.162	0.458

[a] Samples in external test set..

$$EA = E(M) - E(M^-) \quad (7)$$

1.4. Data processing

All statistical analyses were performed using the software package SPSS 22.0. ANOVA method is used to study the influence of the independent variables on the dependent variables. Stepwise regression procedure was used to build QSAR models. The quality of derived QSAR was evaluated in accordance with the squared regression coefficient (R^2), t test and the Fisher test. In order to check the robustness and predictivity of the models, the validation of the final models was performed using leave-one-out cross-validation (Q^2_{LOO}) and the external validation (Q^2_{EXT}) (Li et al., 2013; Sudhakaran and Amy, 2013). In both validation methods, a validation value of greater than 0.5 indicates a robust and predictive model (Eriksson et al., 2003; Ma et al., 2010).

The Q^2_{LOO} and Q^2_{EXT} were calculated as:

$$Q^2_{LOO} = 1 - PESS/TCSS \quad (8)$$

$$Q^2_{EXT} = 1 - \sum_{i=1}^{test}(y_i - \hat{y}_i)^2 \Big/ \sum_{i=1}^{test}(y_i - \bar{y}_i)^2 \quad (9)$$

where PESS is predicted error of sum of squares, TCSS is the total corrected sum of squares. y_i and $\hat{y}_i$ are the measured and predicted k_1 values, respectively. y_i is the averaged value of the k_1 for the training set.

2. Results and discussion

2.1. Meta-analysis of k_1 values

The photodecolorization of the 22 dyes followed the pseudo-first-order kinetics with R^2 values generally larger than 0.96 (Table 2). In order to explore the differences in the photochemical properties of the azo and hydrazone tautomers as well as the possible steric hindrance effect, all the dyes were classified into four categories based on the functional groups: aminoazo and hydroxyazo dyes, with (w/) or without (w/o) sulfonate adjacent to the azo bond (2-sulfo) (Fig. 2a). Hydroxyazo dyes w/o 2-sulfo exhibited statistically different photolysis reactivity ($p < 0.01$). At pH 6.0, the w/o 2-sulfo hydroxyazo dyes (median $k_1 = 0.014\ min^{-1}$) were easier to photolysis than the w/o 2-sulfo aminoazo dyes (median $k_1 = 0.002\ min^{-1}$). The w/ 2-sulfo hydroxyazo dyes exhibited a higher photostability ($k_1 = 0.004\ min^{-1}$) than the w/o counterparts. These statistical features were also applicable at pH 4.0 and pH 9.0 (Fig. 2b and 2c). Hydroxyazo dyes mainly exist in the hydrazone form in aqueous solution (polar and hydrogen bonding environment) and aminoazo dyes primarily exist as azo tautomers (Ball and Nicholls, 1982). The results suggest that the hydrazone tautomer was easier to be photolyzed than the azo tautomer and the 2-sulfo substitution had a significant protective effect on the photodegradation of azo dyes, which was consistent with a previous study (Omura et al., 1992).

Depending upon the conjugated aromatic rings in the molecule, the monoazo dyes could also be classified as: naph-azo-naph, naph-azo-ph, ph-azo-ph dyes. As shown in Fig. 2d, with the increase of conjugation, the photolysis of monoazo dyes became easier.

Table 2 – The pseudo-first order photodegradation rate constant (k_1) of dyes at three pH conditions.

Dyes	CAS	k_1 (min^{-1})		
		pH 4.0	pH 6.0	pH 9.0
Bismarck Brown Y	10114-58-6	1.0E-03	2.8E-03	1.2E-02
Congo Red	573-58-0	1.3E-02	8.4E-03	1.2E-02
Acid Red 73	5413-75-2	3.3E-03	8.6E-04	1.1E-03
Naphthol Blue Black	1064-48-8	6.7E-03	2.7E-03	4.4E-03
Ponceau S	6226-79-5	3.0E-03	1.2E-03	2.4E-03
Chrysoidine	532-82-1	1.9E-03	1.9E-03	4.2E-03
Gold Orange	547-58-0	3.7E-03	1.5E-03	1.8E-03
Orange IV	554-73-4	1.8E-03	2.0E-03	3.2E-03
Mordant Black 11[a]	1787-61-7	9.0E-03	1.3E-02	3.2E-02
Mordant Black 17	2538-85-4	1.0E-01	3.2E-02	1.5E-01
Acid Orange 7	633-96-5	1.9E-02	1.4E-02	3.5E-03
Acid Orange 20	523-44-4	1.7E-02	1.1E-02	2.4E-02
Calconcarboxylic Acid	3737-95-9	5.9E-02	4.3E-02	5.4E-02
Chlorophosphonazo III	1914-99-4	2.3E-03	2.4E-03	5.9E-03
Brilliant Red 5SKH[a]	17804-49-8	1.9E-03	1.2E-03	1.9E-03
Fast Fuchsine G	4197-07-3	3.0E-03	1.9E-03	2.5E-03
Acid Chrome Blue K	3270-25-5	3.1E-03	2.5E-03	1.6E-02
Amaranthe	915-67-3	2.1E-02	1.5E-02	7.6E-03
Bordeaux Red	5858-33-3	1.3E-02	8.9E-03	8.0E-03
Acid Red 26[a]	3761-53-3	1.3E-02	8.1E-03	9.2E-03
Acid Orange 10	1936-15-8	5.5E-03	1.8E-03	1.8E-03
Ponceau 4R	2611-82-7	9.7E-03	2.8E-03	7.9E-03

[a] Samples in external test set.

The effect of pH on the photodegradation of azo dyes was also explored. Fig. 3 shows that the pH-stability of each azo dyes. 13 of 22 dyes are acid and base labile (both $k_{1,\ pH\ 4.0}/k_{1,\ pH\ 6.0}$ and $k_{1,\ pH\ 9.0}/k_{1,\ pH\ 6.0} > 1$). The remaining dyes are either acid ($k_{1,\ pH\ 4.0}/k_{1,\ pH\ 6.0} > 1$) or base ($k_{1,\ pH\ 9.0}/k_{1,\ pH\ 6.0} > 1$) unstable. These results suggest that for a particular azo dye, it is easier to photolysis under acidic and alkaline conditions than that in neutral.

2.2. Model development

All the 16 micromolecular descriptors (i.e. PSA, α, E_{HOMO}, E_{LUMO}, E_{GAP}, μ, EA, IP, EA, η, s, ζ, ω, qC^+, qC^-, qH^+, qH^-) used in model development were calculated. The optimal geometries of Congo Red, Ponceau S, Naphthol Blue Black and Chlorophosphonazo III were not found because of the complexity of structure and the difficulty in computing. Except for these 4 dyes, the dataset was randomly divided into a training set (15 dyes) for developing the QSAR model and a test set (3 dyes) for external validation.

The E_{GAP} could reflect the excitation energy (the lowest electronic transition accessible via absorption of a single photon) (Bredas, 2014). E_{GAP} values of seventy model azo compounds with different substituted groups (-OH, $-NH_2$, $-SO_3^-$, $-NO_2$) and position were constructed and calculated (Fig. 4). These model azo compounds could be classified into three core structures: azo, *o*-hydrazone and *p*-hydrazone. Regardless of the substituent groups and positions, the E_{GAP} values of all azo tautomers were significantly higher than

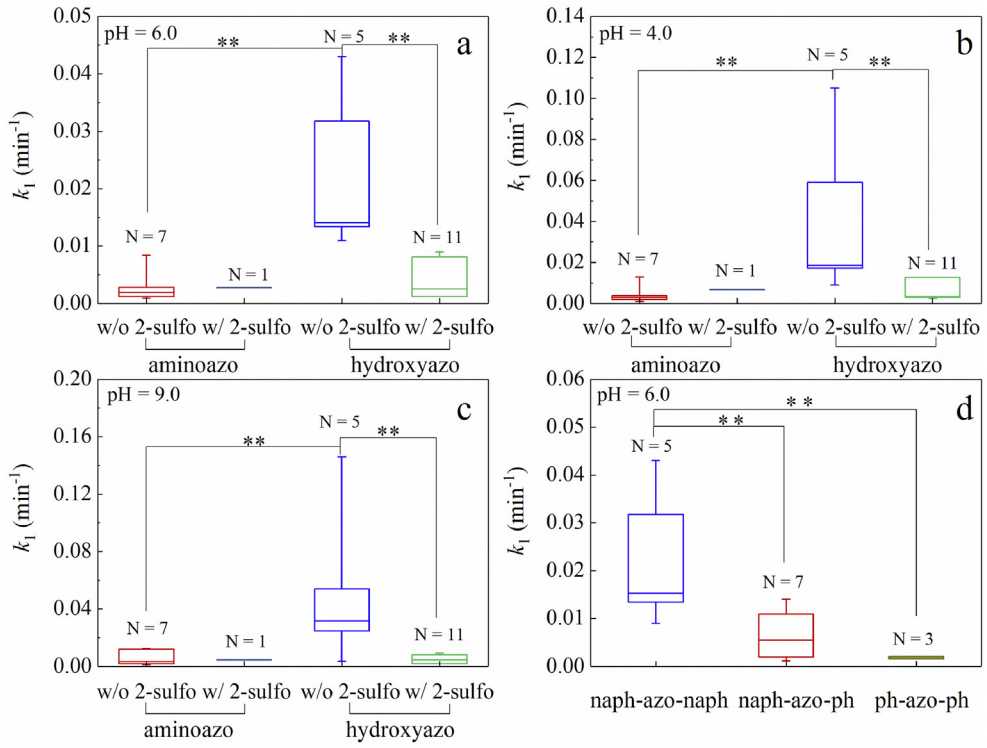

Fig. 2 – Box plots of the pseudo-first order degradation rate constants (k_1) of dyes under UV irradiation (a–c) Grouped by the functional group, (d) Grouped by conjugated carbon skeleton $[dye]_0 = 0.1$ mmol/L, light intensity: 7.89 mW/cm^2 ** represents statistically significant ($p < 0.01$) in one-way ANOVA analysis.

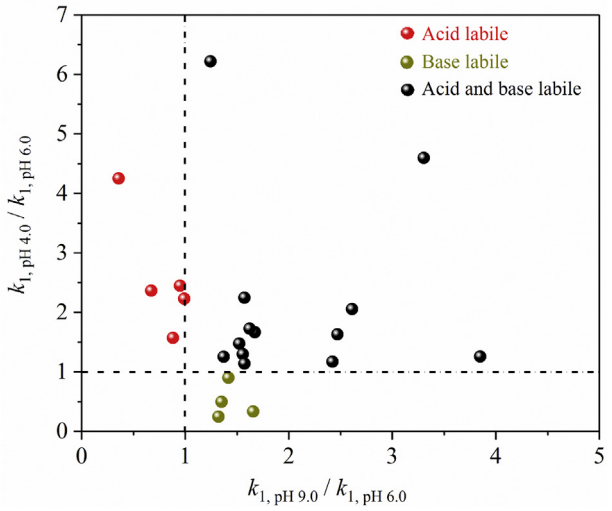

Fig. 3 – The acid/base lability of the dyes judged by the k_1 ratios at different pH.

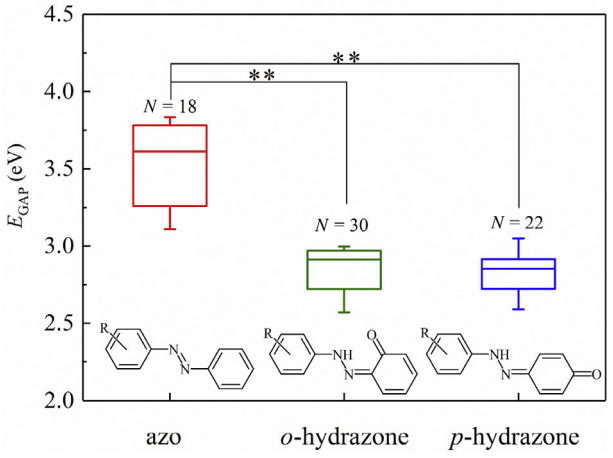

Fig. 4 – Box plot of E_{GAP} values of model azo compounds of three categories. –R represents –OH, –NH_2, –SO_3^-, and –NO_2. **represents statistically significant ($p < 0.01$) in one-way ANOVA analysis.

those of hydroxyazo tautomers. The excitation energies explained why the hydrazone tautomers were easier to be photolyzed than the azo tautomers.

Correlation analysis was conducted between all the descriptors and the k_1 values. There were 6 out of 16 descriptors which exhibited correlation coefficients (r) above 0.5 for the k_1 dataset (Table 3). At the three pHs (4.0, 6.0, 9.0), E_{GAP} and η had strong negative correlation with the k_1 values, while both qC^- and s had strong positive correlation. qC^+ correlated well with the k_1 dataset at pH 4.0 or 9.0, ω correlated well with the k_1 dataset at pH 6.0. The correlations for the k_1 values at initial pHs of 4.0, 6.0 and 9.0 were very strong ($r > 0.7$), indicating that compared to the molecule structure, the solution pH was not the main determining factor in the photodegradation of dyes.

Table 3 – The correlation coefficient between the selected descriptors and the k_1 values.

	$k_{1,\ pH\ 4.0}$	$k_{1,\ pH\ 6.0}$	$k_{1,\ pH\ 9.0}$
$k_{1,\ pH\ 4.0}$	1.000	0.870**	0.957**
$k_{1,\ pH\ 6.0}$	0.870**	1.000	0.728**
$k_{1,\ pH\ 9.0}$	0.957**	0.728**	1.000
E_{GAP}	−0.654*	−0.656**	−0.630*
qC^-	0.738**	0.523*	0.821**
qC^+	−0.678**	−0.326	−0.725**
ω	0.472	0.556*	0.374
s	0.731**	0.741**	0.694**
η	−0.675*	−0.675**	−0.647**

* Statistically significant at $p < 0.05$ level in paired t tests.
** Statistically significant at $p < 0.01$ level in paired t tests.

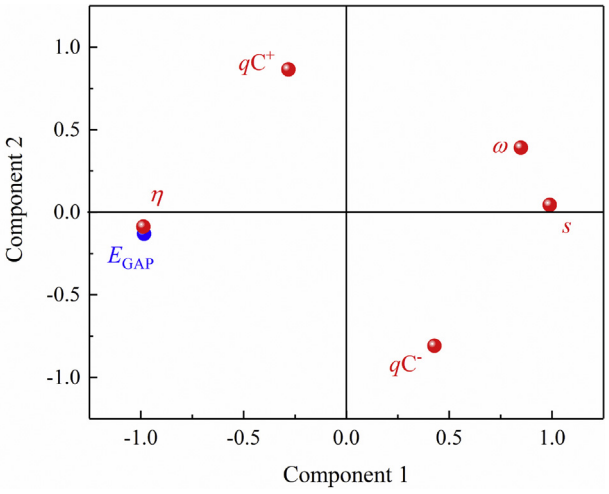

Fig. 5 – Loading plots of the k_1 data set. Component 1 is dominated by s, ω, E_{GAP}, η. Component 2 is dominated by qC^+ and qC^-.

After correlation analysis, PCA was conducted to further reduce the dimensionality of the selected descriptors and to determine the most important variables for k_1. Two principal components were found to account for 91.4% explanation of the total variance. As illustrated in Fig. 5, component 1 was dominated by s, ω, E_{GAP}, η. However, the E_{GAP} and η clustered together, which would cause redundancy in accounting for the variability because of their statistical collinearity. Therefore, s and E_{GAP} were selected to represent component 1, as they have the higher loading score. Component 2 were mostly dominated by qC^+ and qC^-. With the 4 descriptors (i.e., s, E_{GAP}, qC^+ and qC^-) selected in PCA, 3 QSAR equations were obtained using the stepwise MLR method at three pHs. Due to the poor statistical performance, E_{GAP} was excluded in MLR analysis.

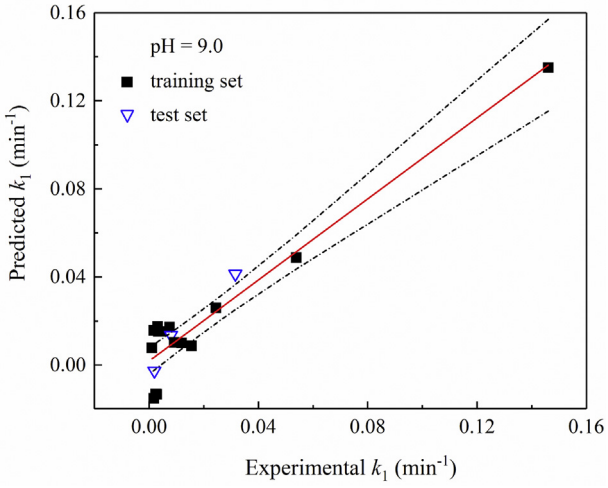

Fig. 6 – Predicted versus experimental k_1 values for the training data and test data at pH 9.0. The dotted lines represent the 95% confidence interval.

The statistical criteria for a good model, including R^2, F, p, and VIF, were met in the second eq (Table 4). The p value was less than 0.05, indicating that it was unlikely that these k_1 values would be observed under the null hypothesis. Further, with the high F value, the null-hypothesis could be eliminated. The VIF less than 10 indicates that the descriptors were not strongly correlated with each other. Among the three QSAR models, the models at pH 4.0 and 9.0 had high goodness of fit ($R^2_{pH\ 4.0} = 0.78$, $R^2_{pH\ 9.0} = 0.88$). The different R^2 values at pH of 4.0, 6.0 and 9.0 might be ascribed to the small sample size and the inaccurate molecular structures of the input model. In fact, in order to explore the effect of solution pH, all of the protonated and deprotonated species of azo dye need to be considered in detail in quantum chemical calculation and model building. However, because of the high calculation cost, it was not explored further in the present work.

In the validation process, the Q^2_{LOO} values at pH 4.0, and 6.0 were 0.5 and 0.3, respectively. The Q^2_{EXT} values at pH 4.0 and 6.0 were all below 0.5. These data indicates that the models at pH 4.0 and 6.0 had instability and poor predictability. The Q^2_{LOO} and Q^2_{EXT} values at pH 9.0 were 0.5 and 0.8, respectively, indicating a good prediction for the model at pH 9.0. The experimental and QSAR predicted k_1 values at pH 9.0 for the internal and external data sets were compared in Fig. 6. Both datasets were in good agreement.

The three QSAR models indicate that the global molecular property descriptor s, which was successful in the interpretation of site-selectivity and/or regiochemistry (Gázquez, 1998; Roy et al., 1998; Torrent-Sucarrat et al., 2010), was proportional to the k_1 values. As for the two molecular

Table 4 – QSAR models established from stepwise multiple linear regression.

Equation	R^2	F	p	VIF	Q^2_{LOO}	Q^2_{EXT}
$k_{1,\ pH\ 4.0} = -0.092 + 0.025(qC^-) + 0.315(s)$	0.78	21	0.01	1.2	0.5	−1.9
$k_{1,\ pH\ 6.0} = -0.074 + 0.194(s)$	0.51	16	0.02	1.0	0.3	−1.8
$k_{1,\ pH\ 9.0} = -0.095 + 0.025\ (qC^-) + 0.366\ (s) - 0.027(qC^+)$	0.88	36	0.01	2.2	0.5	0.8

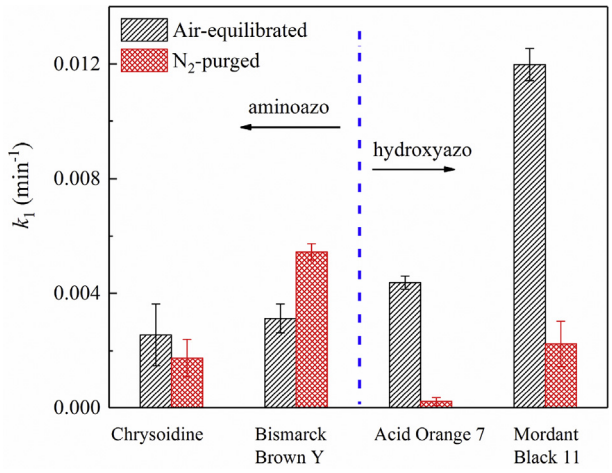

Fig. 7 – The k_1 values of two aminoazo dyes and two hydroxyazo dyes under air-equilibrated and N_2-purged conditions $[dye]_0 = 0.1$ mmol/L, pH: 6.0, light intensity: 7.92 mW/cm^2.

electrostatic interaction descriptors (qC^+ and qC^-), qC^- was positively proportional to $k_{1,\ pH\ 4.0}$ and $k_{1,\ pH\ 9.0}$, while qC^+ was negatively proportional to $k_{1,\ pH\ 9.0}$. These results suggest that the photodegradation of dyes was related to electrophilic reactions.

2.3. *Photo-oxidation mechanism*

Photo-oxidation occurs mainly in the presence of oxygen (O_2), usually irreversible, which involve singlet oxygen ($^1O_2$), superoxide ion ($O_2^{\bullet-}$), and some other reactive oxygen species (ROS) (Kuramoto and Kitao, 1982a, 1982b). To evaluate the role of O_2, two aminoazo dyes (Chrysoidine, Bismarck Brown Y), two hydroxyazo dyes (Acid Orange 7, Mordant Black 11) were selected and the experiments were conducted under UV/N_2 irradiation. N_2-purging had little effect on the photodegradation of Chrysoidine and slightly increased the k_1 value of Bismarck Brown Y (Fig. 7). However, the elimination of O_2 significantly inhibited the photolytic reactions for the hydroxyazo dyes. The k_1 values of Acid Orange 7 and Mordant Black 11 were about 95% and 81%, respectively, inhibited by N_2-purging. These results indicate that O_2 played a decisive role in photodegradation of hydroxyazo dyes.

$^1O_2$ could be generated via energy transfer between the excited azo dyes with O_2. The hydrazone tautomer was proposed as the most likely sensitizer for the production of $^1O_2$ by 4-arylazo-1-naphthols and 1-arylazo-2-naphthols (Griffiths and Hawkins, 1977). The generated $^1O_2$ could either decompose the hydroxyazo dyes through a concerted "ene" mechanism ($^1O_2$ adds to the carbon atom of the C=N group in the hydrozone tautomer) and a hydrogen abstraction from N or quenched by the dyes (Griffiths and Hawkins, 1977). Jansen et al. reported that the contribution of the $^1O_2$ to the photodecomposition of 1-arylazo-2-naphthols in methanol was in the range of 10%–30% (Jansen et al., 1999).

Besides energy transfer, electron transfer might occur between the excited dyes and O_2, leading to the formation of $O_2^{\bullet-}$. $O_2^{\bullet-}$ could undergo various reactions, such as disproportionation, one-electron transfer, and nucleophilic substitution (Hayyan et al., 2016). The disproportionation of $O_2^{\bullet-}$ generates H_2O_2, which could then photolyzed to hydroxyl radicals (•OH). The principal reactions of peroxy radicals and peroxides are hydrogen atom abstraction, addition to unsaturated systems, radical displacement, and oxygen atom transfer (Ingold, 1969). All of the above species might contribute to the photodegradation of the azo dyes. However, due to the complexity of the reaction process, it is difficult to identify the main contributing species.

Meta-analysis shows that there existed a significant protective effect of 2-sulfo (o-SO_3^-) in the hydrazone tautomers. The protective effect of 2-sulfo could be explained from two aspects. First, the negative charge of SO_3^- inhibited the attack of $O_2^{\bullet-}$ through electrostatic repulsion. Second, SO_3^- generated a steric hindrance and thus a reduced accessibility. According to the associated hard/soft acid/base principle (Torrent-Sucarrat et al., 2010), species containing readily polarized oxygen atoms and unpaired electrons are easier to react with the highly polarizable and soft dyes. $^1O_2$, $O_2^{\bullet-}$, •OH and peroxides are such kind of ROS, which explains the positive correlation between the descriptor (*s*, $qC+$ and $qC-$) and the k_1 values in the established QSAR models.

3. Conclusions

Our QSAR model shows that *s*, qC^+ and qC^- could be used to predict the light stability of azo dyes. Internal and external validations indicate that the QSAR model at pH 9.0 had a good predictability and was robust. The three parameters in the QSAR model describe the electrostatic interactions between photoinduced free radicals and azo dyes. N_2-purging experiments and quantum chemical computation verified the speculation obtained from the QSAR models. The experimental and simulation results demonstrate that the photodegradation of azo dyes was not a result of direct photolysis but was caused by the attack of ROS. More research efforts are needed to clarify why the QSAR models at pH 4.0 and 6.0 were not robust enough. The correlation between the speciation of dye molecules and the k_1 values is a topic deserve further research.

Declaration of interests

The authors declare that they have no known competing financial interests or personal relationships that could have appeared to influence the work reported in this paper.

Acknowledgments

This work was financially supported by the National Natural Science Foundation of China (Nos. 21522702, 21677070). The work was also supported by the program B for Outstanding PhD candidates of Nanjing University. We thank the High-Performance Computing Center of Nanjing University for the IBM Blade cluster system.

REFERENCES

Abo-Farha, S.A., 2010. Comparative study of oxidation of some azo dyes by different advanced oxidation processes: Fenton, Fenton-like, photo-Fenton and photo-Fenton-like. J. Am. Sci. 6 (10), 128–142.

Al-Kdasi, A., Idris, A., Saed, K., Guan, C.T., 2004. Treatment of textile wastewater by advanced oxidation processes-a review. Global NEST J 6 (3), 222–230.

Anwer, H., Mahmood, A., Lee, J., Kim, K.H., Park, J.W., Yip, A.C.K., 2019. Photocatalysts for degradation of dyes in industrial effluents: opportunities and challenges. Nano Res. 12 (5), 955–972.

Ball, P., Nicholls, C.H., 1982. Azo-hydrazone tautomerism of hydroxyazo compounds-a review. Dyes Pigm. 3 (1), 5–26.

Basheer, B., Robert, T.M., Vijayalakshmi, K.P., Mathew, D., 2018. Solar cells sensitized by push-pull azo dyes: dependence of photovoltaic performance on electronic structure, geometry and conformation of the sensitizer. Int. J. Ambient Energy 39 (5), 433–440.

Beiknejad, D., Chaichi, M.J., 2014. Estimation of photolysis half-lives of dyes in a continuous-flow system with the aid of quantitative structure-property relationship. Front. Env. Sci. Eng. 8 (5), 683–692.

Berkowitz, M., Parr, R.G., 1988. Molecular hardness and softness, local hardness and softness, hardness and softness kernels, and relations among these quantities. J. Chem. Phys. 88 (4), 2554–2557.

Bredas, J.L., 2014. Mind the Gap. Mater. Horiz. 1 (1), 17–19.

Brode, W.R., Gould, J.H., Wyman, G.M., 1952. The relation between the absorption spectra and the chemical constitution of dyes. XXV. Phototropism and *cis-trans* isomerism in aromatic azo compounds1. J. Am. Chem. Soc. 74 (18), 4641–4646.

Chan, S.H.S., Yeong Wu, T., Juan, J.C., Teh, C.Y., 2011. Recent developments of metal oxide semiconductors as photocatalysts in advanced oxidation processes (AOPs) for treatment of dye waste-water. J. Chem. Technol. Biotechnol. 86 (9), 1130–1158.

Chen, J.W., Kong, L.R., Zhu, C.M., Huang, Q.G., Wang, L.S., 1996. Correlation between photolysis rate constants of polycyclic aromatic hydrocarbons and frontier molecular orbital energy. Chemosphere 33 (6), 1143–1150.

Chen, J.W., Peijnenburg, W.J.G.M., Quan, X., Chen, S., Martens, D., Schramm, K.W., Kettrup, A., 2001. Is it possible to develop a QSPR model for direct photolysis half-lives of PAHs under irradiation of sunlight? Environ. Pollut. 114 (1), 137–143.

Chen, J.W., Peijnenburg, W.J.G.M., Quan, X., Yang, F.L., 2000. Quantitative structure-property relationships for direct photolysis quantum yields of selected polycyclic aromatic hydrocarbons. Sci. Total Environ. 246 (1), 11–20.

Chen, X.Q., Wu, Z.S., Liu, D.D., Gao, Z.Z., 2017. Preparation of ZnO photocatalyst for the efficient and rapid photocatalytic degradation of azo dyes. Nanoscale Res. Lett. 12 (1), 143.

Chung, K.T., 2016. Azo dyes and human health: a review. J. Environ. Sci. Health, Part C 34 (4), 233–261.

Coen, J.J.F., Smith, A.T., Candeias, L.P., Oakes, J., 2001. New insights into mechanisms of dye degradation by one-electron oxidation processes. J. Chem. Soc., Perkin Trans. 2 (11), 2125–2129.

Ekmekci, M., Ela, C., Erten-Ela, S., 2019. Morphological characterization of aluminum-doped zinc oxide nanomaterials (AZO) for dye-sensitized solar cells. Int. J. Appl. Ceram. Technol. 16 (2), 727–734.

Eriksson, L., Jaworska, J., Worth, A.P., Cronin, M.T., McDowell, R.M., Gramatica, P., 2003. Methods for reliability and uncertainty assessment and for applicability evaluations of classification-and regression-based QSARs. Environ. Health Perspect. 111 (10), 1361–1375.

Frisch, M.J.T., Trucks, G.W., Schlegel, H.B., Scuseria, G.E., Robb, M.A., Cheeseman, J.R., et al., 2010. Gaussian 09, Revision B.01. Gaussian, Inc., Wallingford CT.

Gázquez, J.L., 1998. A hardness and softness theory of bond energies and chemical reactivity. In: Párkányi, C. (Ed.), Theoretical and Computational Chemistry. Elsevier, pp. 135–152.

Griffiths, J., Hawkins, C., 1977. Oxidation by singlet oxygen of arylazonaphthols exhibiting azo-hydrazone tautomerism. J. Chem. Soc., Perkin Trans. 1 (6), 747–752.

Haag, W.R., Mill, T., 1987. Direct and indirect photolysis of water-soluble azodyes: kinetic measurements and structure-activity-relationships. Environ. Toxicol. Chem. 6 (5), 359–369.

Hayyan, M., Hashim, M.A., AlNashef, I.M., 2016. Superoxide ion: generation and chemical implications. Chem. Rev. 116 (5), 3029–3085.

Ingold, K.U., 1969. Peroxy radicals. Acc. Chem. Res. 2 (1), 1–9.

Jansen, L.M.G., Wilkes, I.P., Wilkinson, F., Worrall, D.R., 1999. The role of singlet molecular oxygen in the photodegradation of 1-arylazo-2-naphthols in methanol and on cotton. J. Photochem. Photobiol. A Chem. 125 (1–3), 99–106.

Katsumata, H., Koike, S., Kaneco, S., Suzuki, T., Ohta, K., 2010. Degradation of Reactive Yellow 86 with photo-Fenton process driven by solar light. J. Environ. Sci. 22 (9), 1455–1461.

Kuramoto, N., Kitao, T., 1982a. Contribution of singlet oxygen to the photofading of some dyes. J. Soc. Dyers Colour. 98 (10), 334–340.

Kuramoto, N., Kitao, T., 1982b. Contribution of superoxide ion to the photofading of dyes. J. Soc. Dyers Colour. 98 (5–6), 159–162.

Lee, C., Yang, W., Parr, R.G., 1988. Development of the colle-salvetti correlation-energy formula into a functional of the electron density. Phys. Rev. B 37 (2), 785.

Li, B., Dong, Y.C., Ding, Z.Z., 2013. Heterogeneous Fenton degradation of azo dyes catalyzed by modified polyacrylonitrile fiber Fe complexes: QSPR (quantitative structure peorperty relationship) study. J. Environ. Sci. 25 (7), 1469–1476.

Ma, B., Chen, H., Xu, M., Hayat, T., He, Y., Xu, J., 2010. Quantitative structure-activity relationship (QSAR) models for polycyclic aromatic hydrocarbons (PAHs) dissipation in rhizosphere based on molecular structure and effect size. Environ. Pollut. 158 (8), 2773–2777.

Ma, R., Zhang, S., Wen, T., Gu, P.C., Li, L., Zhao, G.X., et al., 2019. A critical review on visible-light-response CeO_2-based photocatalysts with enhanced photooxidation of organic pollutants. Catal. Today 335, 20–30.

Mannhold, R., Krogsgaard-Larsen, P., Timmerman, H., 2008. QSAR: hansch analysis and related approaches. John Wiley & Sons.

Marenich, A.V., Cramer, C.J., Truhlar, D.G., 2009. Universal solvation model based on solute electron density and on a continuum model of the solvent defined by the bulk dielectric constant and atomic surface tensions. J. Phys. Chem. B 113 (18), 6378–6396.

Omura, T., Kayane, Y., Tezuka, Y., 1992. Design of chlorine-fast reactive dyes: Part 1: the role of sulphonate groups and optimization of their positions in an arylazonaphthol system. Dyes Pigm. 20 (4), 227–246.

Pandey, A., Singh, P., Iyengar, L., 2007. Bacterial decolorization and degradation of azo dyes. Int. Biodeterior. Biodegrad. 59 (2), 73–84.

Pearson, R.G., 1986. Absolute electronegativity and hardness correlated with molecular orbital theory. Proc. Natl. Acad. Sci. U. S. A. 83 (22), 8440–8441.

Puvaneswari, N., Muthukrishnan, J., Gunasekaran, P., 2006. Toxicity assessment and microbial degradation of azo dyes. Indian J. Exp. Biol. 44 (8), 618–626.

Roy, R.K., Krishnamurti, S., Geerlings, P., Pal, S., 1998. Local softness and hardness based reactivity descriptors for predicting intra- and intermolecular reactivity sequences: carbonyl compounds. J. Phys. Chem. A 102 (21), 3746–3755.

Sato, H., Beppu, I., Haraguchi, T., Akitsu, T., Parida, R., Giri, S., et al., 2018. Optical properties of chiral schiff base Mn-II, Co-II, Ni-II complexes having azobenzene. J. Indian Chem. Soc. 95 (12), 1487–1495.

Soares, P.A., Silva, T.F.C.V., Arcy, A.R., Souza, S.M.A.G.U., Boaventura, R.A.R., Vilar, V.J.P., 2016. Assessment of AOPs as a polishing step in the decolourisation of bio-treated textile wastewater: technical and economic considerations. J. Photochem. Photobiol., A 317, 26–38.

Sudhakaran, S., Amy, G.L., 2013. QSAR models for oxidation of organic micropollutants in water based on ozone and hydroxyl radical rate constants and their chemical classification. Water Res. 47 (3), 1111–1122.

Sztandera, L., Garg, A., Hayik, S., Bhat, K.L., Bock, C.W., 2003. Mutagenicity of aminoazo dyes and their reductive-cleavage metabolites: a QSAR/QPAR investigation. Dyes Pigm. 59 (2), 117–133.

Thanavel, M., Kadam, S.K., Biradar, S.P., Govindwar, S.P., Jeon, B.H., Sadasivam, S.K., 2019. Combined biological and advanced oxidation process for decolorization of textile dyes. Sn Appl. Sci. 1 (1).

Torrent-Sucarrat, M., De Proft, F., Ayers, P.W., Geerlings, P., 2010. On the applicability of local softness and hardness. Phys. Chem. Chem. Phys. 12 (5), 1072–1080.

van Beek, H.C.A., Heertjes, P.M., 1963. Photochemical reactions of azo dyes in solution with different substrates. J. Soc. Dyers Colour. 79 (12), 661–670.

van Beek, H.C.A., Heertjes, P.M., Houtepen, C., Retzloff, D., 1971. Formation of hydrazyl radicals and hydrazo compounds by photoreduction of azo dyes. J. Soc. Dyers Colour. 87 (3), 87–92.

Wu, Q.Y., Li, Y., Wang, W.L., Wang, T., Hu, H.Y., 2016. Removal of CI Reactive Red 2 by low pressure UV/chlorine advanced oxidation. J. Environ. Sci. 41, 227–234.

Xiao, R.Y., Ye, T.T., Wei, Z.S., Luo, S., Yang, Z.H., Spinney, R., 2015. Quantitative structure-activity relationship (QSAR) for the oxidation of trace organic contaminants by sulfate radical. Environ. Sci. Technol. 49 (22), 13394–13402.

Yasar, A., Ahmad, N., Khan, A.A.A., Yousaf, A., 2007. Decolorization of Blue CL-BR dye by AOPs using bleach wastewater as source of H_2O_2. J. Environ. Sci. 19 (10), 1183–1188.

Zhan, C.G., Nichols, J.A., Dixon, D.A., 2003. Ionization potential, electron affinity, electronegativity, hardness, and electron excitation energy: molecular properties from density functional theory orbital energies. J. Phys. Chem. A 107 (20), 4184–4195.

Zhang, G.Y., Wei, S.J., Wu, B.D., Chen, Z.H., Zhang, S.J., 2018. Nonnegligible generation of hydroxyl radicals from UVC photolysis of aqueous nitrous oxide. Environ. Sci. Technol. 52 (17), 9785–9792.